A Low-Cost Smartphone-Based Photogrammetric Approach for Highway Pavement Defects Detection and Mapping

Mohand Oussaid, F.,[1,5*] Raham, D.,[2] Boukerch, I.,[3] Mezhoud, S.,[1] Saidi, K.[4] and Kariche, I.[5]
[1]FSTGAT, Frères Mentouri University Constantine1, Constantine, Algeria
E-mail: farid.mohandoussaid@doc.umc.edu.dz,* mezhoud.sami@umc.edu.dz
[2]Research Center in Spatial Planning, CRAT, Constantine, Algeria E-mail: raham.djamel@crat.dz
[3]Space Applications Center, SAC- ASAL, Algiers, Algeria, E-mail: iboukerch@asal.dz
[4]National Higer School of Geodetic Sciences and Space Techniques ENSGTS-ASAL, Arzew, Algeria
E-mail: kamel.saidi@ensgts.dz
[5]Mohamed Ben Ahmed University Oran2, Oran, Algeria, E-mail: kariche.ismahane@univ-oran2.dz
**Corresponding Author*

DOI: https://doi.org/10.52939/ijg.v21i11.4601

Abstract

Evaluating the condition of the pavement is a crucial step before undertaking any maintenance or rehabilitation work. This study presents an innovative low-cost smartphone-based workflow that leverages photogrammetric techniques for mapping and measuring pavement surface defects, specifically designed to overcome the limitations of existing UAV (Unmanned Aerial Vehicle) and LiDAR (Light Detection and Ranging) based inspection methods, including high costs, operational complexity, and regulatory or environmental constraints. Unlike existing smartphone-based approaches that primarily focus on defect detection or classification, this method enables both accurate geolocation and precise measurement of key defect dimensions (length, width, and area), generating georeferenced frames interpretable through Geographic Information Systems (GIS). The workflow relies on a Redmi 9 smartphone and its integrated sensors, including camera, accelerometer, gyroscope, magnetometer and GPS (Global Positioning System) combining video capture and GPS/IMU (IMU, Inertial Measurement Unit) recording to produce georeferenced data suitable for GIS analysis. The system was tested on a section of the East-West Highway (from Kilometer Point 150 to 193, in Mila and Constantine provinces, Algeria), driven at a cruising speed of 70 km/h. Compared to a reference survey conducted in situ with a Global Navigation Satellite System (GNSS) receiver (Garmin GPSmap 62s), the results demonstrated high performance, with an F1 score of 93.27%. The system proved effective in detecting and mapping the main surface defects, such as longitudinal and transverse cracks, alligator cracking, and rutting. This novel smartphone-based workflow provides a cost-effective, rapid, and operationally flexible solution for road maintenance planning, enabling targeted and optimized interventions. Particularly useful in developing countries, this method allows for cyclic inventories of road infrastructure with a modest budget while maintaining reliability and accessibility.

Keywords: GIS, GPS, Pavement Defect, Photogrammetry, Smartphone

1. Introduction

Algeria, with its vast and diverse territory, has an extensive road network that plays a crucial role in the country's socio-economic development. However, managing, maintaining, and assessing this network presents significant challenges [1], both technically and logistically. A major complexity lies in the inability to conduct a comprehensive diagnosis of road conditions within a short time frame and on a large scale.

Although the acquisition of specialized vehicles equipped with cutting-edge technologies such as scanners, cameras, GPS, and ground-penetrating radar is feasible, their widespread implementation on a national scale remains unrealistic due to their high cost and limited availability [2]. As a result, in the context of a developing country, Algeria continues to rely primarily on traditional inspection methods [3], which are mostly visual and manual.

However, these methods are time-consuming, costly, prone to human error, and, most importantly, expose personnel to increased risks associated with traffic and environmental conditions. In light of these limitations, exploring more accessible and secure alternative solutions [4] and [5] becomes imperative. Among these alternatives, the use of smartphones for collecting and analyzing road data emerges as a promising solution. Equipped with embedded sensors such as accelerometers [6], GPS, and other technologies, smartphones can contribute to more efficient, rapid, and cost-effective monitoring of road infrastructure conditions, while addressing national budgetary constraints. This innovative approach offers a viable compromise between technological accessibility, operator safety, and diagnostic efficiency.

Unlike recent technological approaches based on UAVs or LiDAR sensors, the present study introduces a low-cost photogrammetric workflow relying on a smartphone, specifically designed for rapid and safe assessment of highway surfaces. This solution aims to balance accuracy, deployability, and speed, while reducing the material and operational constraints commonly associated with conventional inspection systems. It therefore represents an economical and flexible alternative for the mapping and measurement of pavement defects under real traffic conditions, contributing to a more practical and field-adapted inspection process. This study focuses on optimizing the use of low-cost smartphone-based technology for comprehensive road defect monitoring by combining deep learning methods with photogrammetric techniques and GPS technology. This integration enables the identification, classification, and accurate measurement of key dimensions, such as width, length, and area, while ensuring precise geolocation of defects. By offering a more affordable and effective alternative to costly systems, this approach not only improves road infrastructure monitoring and management but also facilitates the estimation of material quantities for repairs, prioritization of interventions, and tracking of damage progression over time. Furthermore, it allows the creation of detailed geospatial databases, enhancing decision-making processes and promoting more efficient resource management

1.1 Related Works

As highlighted earlier, traditional methods of road condition monitoring are time-consuming, costly, and prone to human error. To overcome these limitations, recent studies have explored a range of innovative technologies aimed at improving the efficiency and cost-effectiveness of road defect detection. Among these advancements, automatic detection systems have gained particular attention for their potential to facilitate timely interventions and optimize maintenance planning.

Road surface defect detection remains a significant challenge in transportation infrastructure monitoring. While regular inspections are essential for ensuring road safety, conventional methods are often manual and labor-intensive, which makes them costly and inefficient. To address these issues, various sensing technologies and data-driven approaches have emerged in recent years [7] and [8]. For example, a recent study [9] introduced an efficient road crack detection technology based on YOLOv8-ES, demonstrating significant improvements in detection speed and accuracy for road surface monitoring. This method complements existing vision-based systems, offering a more reliable solution for real-time crack detection. Vision-based systems are widely used for road condition monitoring [10] and [11], typically employing high-resolution remote sensing images [12], including those captured by drones (Unmanned Aerial Vehicles, UAVs) [13] and [14] or vehicle-mounted cameras. These images are processed using deep learning techniques to detect and classify various types of damage, aligning with advancements [9] in improving detection capabilities. For instance, the study reported in [15] combined UAV imagery with machine learning algorithms to accurately identify pavement deformations, further advancing the potential of vision-based systems and demonstrating the significant role of drones in road condition monitoring. Similarly, according to [16] smartphone cameras were used to capture images of road defects and applied Mask R-CNN to classify and segment these defects, showcasing the effectiveness of widely available mobile technology in road damage detection. In addition to vision-based methods, LiDAR sensors offer another advanced approach for capturing detailed 3D representations of road surfaces. This technique enables the detection of both surface and structural cracks that may not be visible in traditional photographs. [17] introduced a mobile LiDAR system enhanced with machine learning and intensity normalization, yielding accurate crack detection results, which are made accessible through an open-source WebGIS platform. Alongside ground-based systems, satellite remote sensing is increasingly being adopted for large-scale road monitoring. For instance, [18] applied multi-temporal SAR interferometry (InSAR) to detect ground displacements that may affect road integrity, providing a complementary solution for monitoring extensive areas.

Additionally, several studies have investigated the potential of integrating SAR, multispectral, thermal [19], and LiDAR technologies for comprehensive infrastructure monitoring, such as road assessments [20].

Recent studies have emphasized the role of integrated sensor networks and geoinformatics for long-term infrastructure monitoring [21][22] and [23]. In this context, [22] introduces the TRIB Crack dataset, specifically designed for the development of an automatic system for road crack detection. The dataset consists of images captured using a digital camera under natural lighting conditions at various times of the day, providing diverse scenarios to improve crack visibility. This collection of images supports the training of machine learning models designed to accurately detect and classify road surface damage, thereby contributing to more efficient road maintenance. Equipped with multiple sensors such as GPS, cameras, accelerometers, and gyroscopes, smartphones serve as powerful, cost-effective platforms for participatory road monitoring [24]. The growing reliance on smartphones has increasingly directed researchers towards utilizing these devices for various monitoring applications, leading to the creation of several datasets containing images captured by smartphones. [16] introduced the first large public dataset, comprising 9 053 annotated images, representing 15 435 instances of road surface damage, and trained deep neural networks to identify and classify different types of damage from these smartphone images. Since its inception, this image dataset has been further expanded through the contributions of subsequent studies including [25] and [26], ultimately culminating in the RDD2022 dataset [27]. This latest iteration encompasses over 47 420 images from multiple countries, including Japan, India, and the United States, thus offering a diverse and comprehensive resource for advancing automated road damage detection systems. These datasets play a pivotal role in facilitating the training of machine learning models, significantly enhancing the accuracy and scalability of road anomaly detection in real-world environments. Moreover, several researchers have proposed utilizing these devices in image acquisition applications for the identification and classification of road defects. [28] proposed a multimodal system combining smartphone camera data and motion sensors to detect road surface anomalies and measure vehicle acceleration, enabling more accurate assessment of defect severity. [6] developed a smartphone-based CNN model for real-time classification of road defects, including potholes, speed bumps, and manhole covers, using vibration sensors, specifically accelerometers. [23] combined GNSS data with image processing to identify cracks in rigid pavements, achieving results comparable to manual inspections.

These studies highlight how low-cost participatory sensing technologies can complement traditional, more complex monitoring systems. However, UAV- and LiDAR-based inspection techniques, despite their proven accuracy, remain constrained by deployment costs, weather dependence, and regulatory restrictions. In contrast, the proposed approach capitalizes on the synergy between smartphone imaging, photogrammetric processing, and precise georeferencing to provide an accessible, fast, and cost-effective alternative for road defects mapping and measurement. This contribution emphasizes operational flexibility and affordability, positioning the proposed system as a practical solution for large-scale, real-world infrastructure monitoring. The integration of smartphone-based tools offers a practical, scalable solution for democratizing road condition monitoring, particularly in regions with limited access to professional-grade survey equipment.

2. Methodology

This research is based on a process using a low-cost smartphone-based technique (Figure 1) for the automatic detection and classification of road defects, in which a deep learning algorithm was employed.

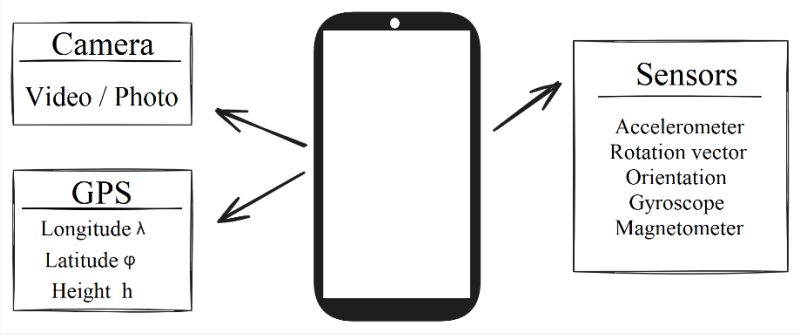

Figure 1: Low-cost smartphone-based technique

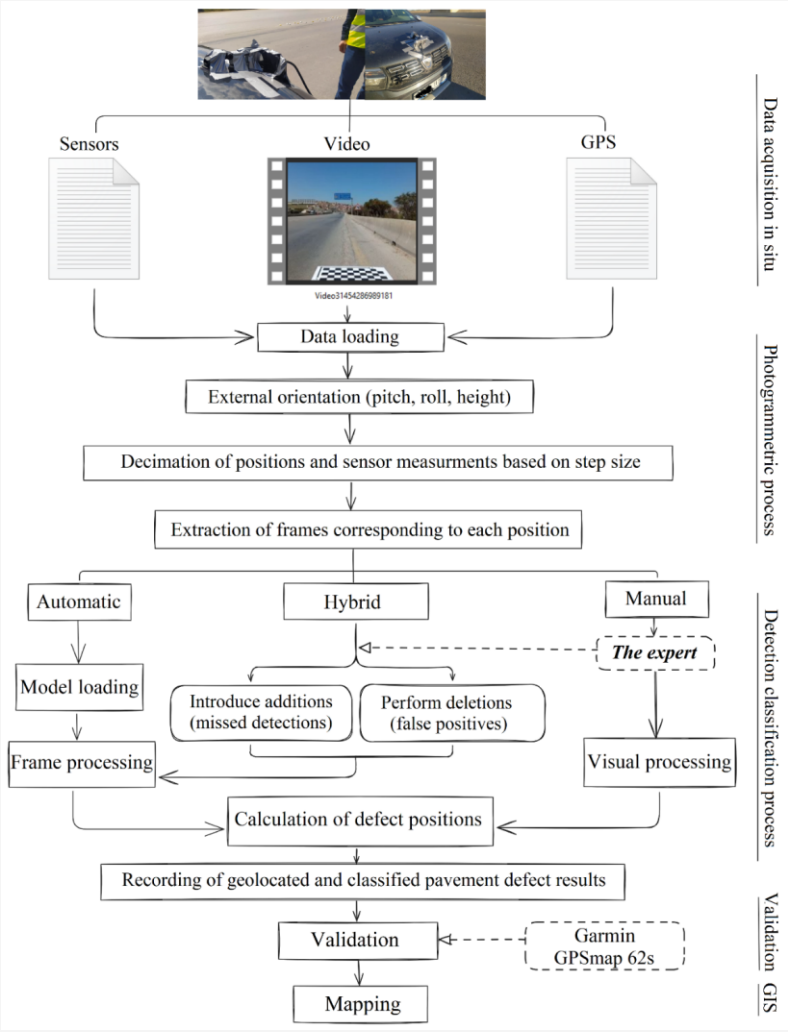

Figure 2: Workflow of the highway pavement defect detection methodology

Table 1: Studied sections

Section	From KP	To KP	Length (km)	Commissioning	Pavement structure
A	150+000	170+000	20.00	2010	semi-rigid
	187+000	193+000	6.00	2011	
B	170+000	187+000	15.36	2006	Flexible

Unlike the studies cited in the previous section, which used similar techniques for road defect detection, the methodology adopted in this study also relies on a photogrammetric approach, integrated into the processing workflow to geolocate the defects, thus enabling the creation of an accurate map depicting the condition of the studied road section at the end of the process. The methodological workflow, illustrated in Figure 2, integrates the synchronized acquisition of data (video, coordinates, and sensor information), followed by photogrammetric processing to assign precise metric properties to the frames. The detected pavement defects are then automatically identified, classified, and geolocated using deep learning. The approach is subsequently validated before producing the final thematic maps of the detected defects.

2.1 Study Area

This study focuses on two distinct sections of the Algerian East-West Highway A1, designated as Sections A and B, located between the Mila and Constantine provinces. The investigated corridor covers a total length of approximately 41.36 km (Table 1) and was constructed by two different companies. As summarized in Table 1 and illustrated in Figure 3, the studied highway segment comprises two structurally different pavement sections.

Section A (shown in blue in Figure 3) corresponds to a semi-rigid pavement opened to traffic between 2010 and 2011, covering two subsections: KP150+000 -170+000 and KP187+000 -193+000 both built by the same contractor. Section B (shown in red) represents a flexible pavement that entered service in 2006, extending from KP170+000 to KP187+000. The visual correspondence between Figure 3 and Table 1 provides a clearer spatial understanding of the two pavement structures, emphasizing the contrast in their service age and structural design. These parameters are critical to explaining the observed differences in surface condition and defect manifestation. The selection of this study area is based on several criteria: a significant difference in pavement structure (semi-rigid for Section A and flexible for Section B), distinct commissioning dates (2011 for Section A and 2006 for Section B), the crossing of varied microclimates, as well as heterogeneity in geological conditions, traffic intensity, and construction methods. These particularities make this area especially relevant for a comparative analysis of pavement behavior in contrasting contexts. A study [29] on a 107 km segment of the A1 highway, located between Setif, Mila, and Constantine, part of which is also included in the present analysis, identified the appearance of longitudinal cracks just a few months after the infrastructure's commissioning in July 2010. A follow-up assessment, conducted over a period of one year starting in November 2010, revealed a continuous deterioration of the road condition. Three years later, further inspections confirmed that these defects had continued to develop and worsen, progressively compromising the strength and overall quality of the pavement. Building upon these findings, a comprehensive visual survey was conducted along the 41.36 km study section to evaluate the pavement condition and identify various forms of defect. This preliminary reconnaissance revealed four major types of deterioration affecting the studied sections: longitudinal cracks, the main type of defect observed; transverse cracks; alligator cracking; as well as rutting and potholes, predominantly located in areas with steep slopes and heavy traffic (Figure 4).

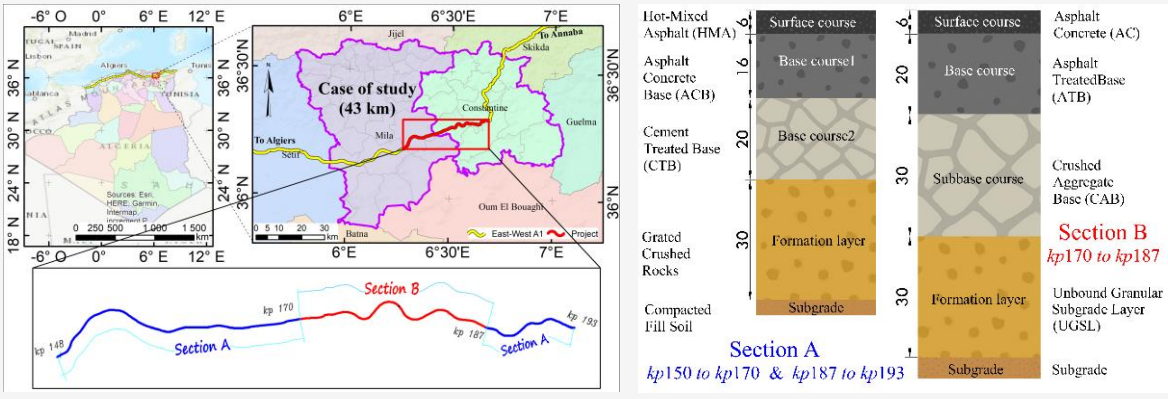

Figure 3: Study area showing Section A (blue, semi-rigid) and Section B (red, flexible) with their respective kilometer points

Figure 4: Principal types of defects affecting the studied sections
(a) longitudinal cracks (b) transverse cracks (c) alligator cracking (d) rutting and pothole

In this context, it is clear that this area is subject to continuous defect, which underscores the importance of implementing a detailed automated survey aimed at geolocating, identifying, and classifying the defects. This approach will contribute to better maintenance management and facilitate decision-making for necessary interventions, ensuring a proactive and efficient strategy.

2.2 Data Acquisition

The collection of the data required for this work was carried out through two main missions: acquisition using a smartphone mounted on a vehicle, and point-based recording of defects with a GPS for validating the approach.

2.2.1 First mission

The field data acquisition mission was carried out in the morning of April 5, 2023, along the corridor of the highway section connecting Constantine to Mila (from KM150 to KM193), covering a total round-trip distance of 82.72 km. The operation was conducted at an average cruising speed of 60 km/h, ensuring an optimal balance between measurement continuity, data readability, and compliance with highway safety conditions. The acquisition system (Figure 5) implemented consisted of a Redmi 9 smartphone equipped with several onboard sensors (GPS, accelerometer, gyroscope, magnetometer), securely mounted on the hood of a Sandero Stepway vehicle using appropriate mechanical supports (Figure 6).

To ensure uniform coverage of the highway platform, which has a total width of 15 meters (comprising three lanes and a shoulder), the vehicle was maintained in the central lane throughout the survey. Data acquisition was performed using an Android application, *Road Recorder*, developed at the Center of Space Techniques (CST, Algeria). The interface of the application is illustrated in Figure 7. *Road Recorder* is specifically designed for multimodal data collection, it captures data in the form of video images, which are essential for research and detecting pavement surface defects. The data are recorded in three files (Figure 8):

- *GPS.txt* file: Dedicated to localization, and structured as follows: ID, Longitude, Latitude, Altitude, Accuracy, Speed, and Time. The recording frequency of this data is one observation per second.
- *Sensors.txt* file: Contains information from the sensors. The measurements taken by these sensors have a sampling time typically of 10 milliseconds.
- *Video* file: A .mp4 format file, which accompanies the recorded data.

The synchronization between the three data files is achieved through the measurement time (Figure 9). To ensure accurate and efficient data collection, prior to each sequence, the smartphone's geolocation feature was activated, ensuring the spatio-temporal synchronization of the recorded information.

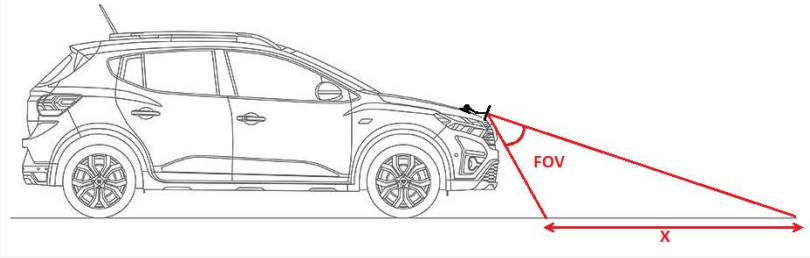

Figure 5: FoV of mobile mapping system

Figure 6: The implemented acquisition system

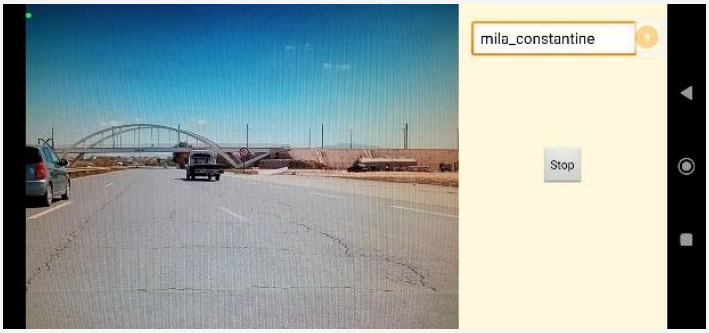

Figure 7: Road recorder interface

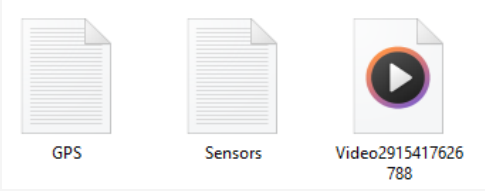

Figure 8: Data files recorded in Road Recorder

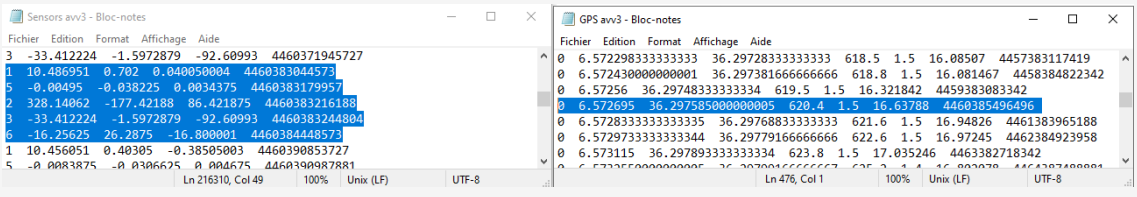

Figure 9: Sensor data synchronized with GPS position

Table 2: data acquisition sequences

Id	Start time	End time	Duration	Distance (km)	Maximum Speed (km/h)	Average Speed (km/h)	Size (GB)	Direction	Departure	Arrival
Avv1	10:40	11:05	$24^{m}\ 09^{s}$	23.92	83.79	59.43	1.68	To Algiers	Smara	Milev
Avv2	11:12	11:37	$24^{m}\ 46^{s}$	28.16	86.93	68.22	1.73	To Annaba	Milev	Smara
Avv3	11:39	12:00	$20^{m}\ 55^{s}$	16.37	76.37	46.97	1.46	To Annaba	Smara	El Khroub
Avv4	12:02	12:21	$18^{m}\ 30^{s}$	16.10	79.41	52.22	1.29	To Algiers	El Khroub	Smara

To manage data volumes more effectively and avoid overloading during processing, the mission was divided into four independent acquisition sequences named Avv1, Avv2, Avv3, and Avv4 as presented in (Table 2). This methodology ensured efficient coverage of the targeted road section while facilitating data storage, exploitation, and post-processing analysis.

2.2.2 Second mission

To evaluate the performance of the photogrammetric model and the reliability of the automatic detections, a total of 140 GPS validation points were collected in situ along the studied highway section, using a mobile GPS unite (Garmin GPSmap 62s) (Figure 10). This number was deliberately limited for reasons of safety, feasibility, and measurement reliability. The survey was carried out on a three-lane highway with a shoulder in each direction, where the speed limit is 120 km/h, frequently exceeded by many drivers. The traffic flow is dense and continuous, making field operations particularly hazardous for inspection and maintenance personnel. To minimize human risk, all validation points were personally surveyed by the author, following strict safety protocols and traffic regulations. Each point required a waiting period to allow for the full initialization of the Garmin GPS receiver, ensuring signal stability and reliable coordinate acquisition. The points were distributed across the full width of the roadway, including the fast lane, in order to achieve spatial representativeness of the different pavement surface conditions.

Longitudinally, the 140 points were uniformly distributed along the 82 km of the studied highway section, corresponding to an average spacing of approximately one reference point every 500 meters. This ratio offers an optimal balance between operator safety, spatial representativeness, and geometric precision. Furthermore, this methodological choice is consistent with established standards in photogrammetric validation studies, where a limited but highly accurate and well-distributed sample is preferred for assessing model performance and large-scale detection accuracy. These points, representing the actual terrain conditions (true defects), were categorized according to different types of pavement defects (D00, D10, D20, and D40). Among them, several points were recorded in defect-free areas of the highway, corresponding to the *ND* (No Defect) *class*.

2.3 Photogrammetric Approach

In the proposed approach, each detected defect is initially located within the image file coordinate system. After a calibration step, the interior and exterior orientation parameters are estimated, which can be done using a checkerboard placed in front of the camera (Figure 11). The primary goal of this step is to locate the camera relative to the vehicle's coordinate system. This allows for the back-projection of the detected defect coordinates onto the road plane in front of the vehicle, passing through the wheel contact points. In a separate test evaluating positioning accuracy, this projection methodology can achieve an accuracy of a few centimeters (±3 cm) for objects located less than 20 meters in front of the camera.

The next stage involves transforming the located defects from the vehicle frame to the local topographic ENU (North East Up) frame and then to the geographic coordinate system. This is achieved by integrating data read from the orientation sensors and the GPS embedded in the smartphone. In this way, each detected defect undergoes a series of transformations to be accurately positioned on the ground (Figure 12). It is important to note that the final accuracy of our setup is around 2.5 to 3 meters, which is due to the accuracy limitations of the devices onboard the smartphone. The use of higher-grade IMUs and RTK GPS could significantly enhance the system's positioning accuracy. Before proceeding to the defect detection and positioning stage, the video undergoes a geo-decimation process. In this process, the GPS file is processed to extract the time corresponding to positions at pre-fixed step (10 meters) from the starting point. Since the GPS file and the video are perfectly synchronized, the image at each step is extracted from the video and forwarded to the detection and positioning stage [30].

Figure 10: Garmin acquisition in situ (GPSmap 62s)

Figure 11: Smartphone camera calibration with Checkerboard Pattern

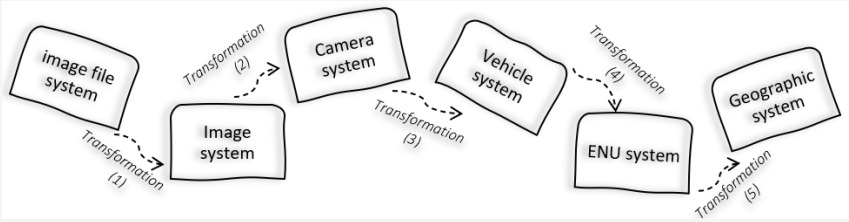

Figure 12: Transition between coordinate systems

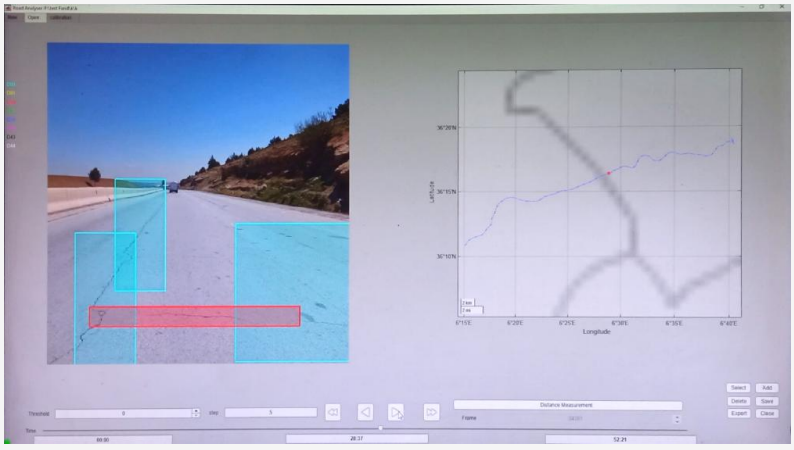

Figure 13: Road Analyzer interface

2.3.1 Detection, classification and geolocation

The recorded data are processed by *Road Analyzer*, an application also developed at CST, which employs a deep learning approach based on Faster R-CNN for the detection and classification of pavement defects. The photogrammetric approach has been integrated into this application to geolocate the defects once they are detected and classified. This allows the output to provide the geographical coordinates λ and φ for each defect. The classification employed in this study is based on [16], where the defect types are denoted by the letter D followed by a numerical identifier. In their study, [16] presented a table comprising eight distinct defect classes. However, the updated dataset (RDD 2022) includes only four defect classes: D00 for Longitudinal Cracks, D10 for Transverse Cracks, D20 for Alligator Cracks, and D40 for Potholes and rutting [27] and [31]. The classification adopted in this work is derived from this updated system (four types). Figure 13 illustrates the Road Analyzer interface, where two types of defects have been detected: D00 in cyan and D10 in red. The position of the frame is indicated by a red dot on the map, located on the right side of the interface.

The performance of the application, evaluated on different datasets, achieved an average F1 score of 77%. To refine the results obtained by the Road Analyzer, the hybrid method adopted in this study relies on the expertise of a domain specialist. Their intervention consists of adding omitted elements or removing erroneous detections.

2.3.2 Validation process

The performance of the photogrammetric approach was evaluated based on the point-based defects recorded during the second acquisition mission. A confusion matrix is calculated, using the following metrics: Recall, Precision, and F1-score [32] , defined in equations 1 to 3. A Python program was developed to automate this computation.

$$Recall = \frac{TP}{TP+FN}$$

Equation 1

$$Precision = \frac{TP}{TP+FP}$$

Equation 2

$$F1\text{-}score = 2\frac{Recall \times Precision}{Recall+Precision}$$

Equation 3

Where:

TP = True Positive
FP = False Positive
FN = False Negative

The process for calculating the confusion matrix and the classification report follows the steps outlined below (Figure 14):

1. For each terrain collected point, a circle with a 10-meter radius is defined. Within this radius, the presence of defects detected by the approach is checked.
2. If a defect is detected within the 10-meter radius, the program identifies its type. If the detected defect type matches the one recorded in the field, the point is counted as a *TP* (True Positive) for that specific defect type. On the other hand, if the detected defect does not match the one recorded, the point is counted as an FP (False Positive) for the detected defect type and as an FN (False Negative) for the expected defect type.
3. If no defect is detected within the 10-meter radius, the point is classified as ND. In this case, if the recorded point represents a defect, it is counted as a FP for the ND class, while if the recorded point is not a defect, it is counted as a TP for the ND class.

2.4 Mapping Approach

A comparative analysis was carried out using advanced Geographic Information Systems (GIS) tools, which integrated spatial analysis, thematic semiology, spatial interpolation, and various geoprocessing operations. This approach enabled the simultaneous examination of both traffic directions, facilitating the identification and characterization of disparities in pavement defect along the highway section. The adopted methodology consists of several stages. First, defects were detected, classified, and georeferenced. The resulting dataset was then exported to the WGS 1984 geographic coordinate system and imported into a GIS environment (ArcGIS). The data were organized into four distinct thematic layers, each corresponding to a specific type of recorded defect. For each layer, a spatial density analysis was conducted using the Kernel Density Estimation (KDE) statistical method. This technique generates continuous surfaces that represent the spatial distribution of defect concentrations along the highway corridor. A 100-meter search radius was applied, serving as an intermediate smoothing parameter that balances local detail with a broader overview on the studied phenomenon.

The calculation is based on summing the weighted contributions of all kernels within the study area, resulting in a smoothed surface that highlights regions of high density (elevated concentrations) and low density. This representation provides a clearer and more analytically meaningful view of spatial distribution compared to a simple overlay of thousands of raw data points. The analyzed highway section extends over approximately 42 km, with a right-of-way ranging between 30 and 35 m in width. The high density of recorded data (over 11,000 defect points) presented a challenge for graphical readability. To enhance visual clarity, a lateral offset was applied (on both sides of the highway axis) to the density bands corresponding to each defect category (Figure 15). The adopted offset distances were as follows: D00 shifted by 600 m, D10 shifted by 900 m, D20 shifted by 1200 m, and D40 shifted by 1500 m.

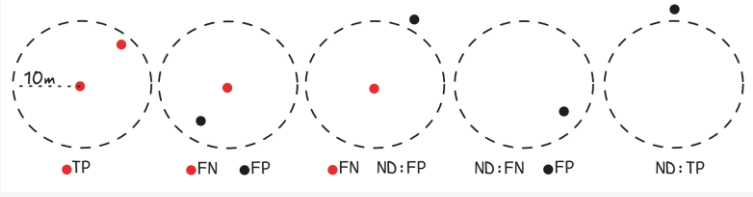

Figure 14: Example of the validation process calculation

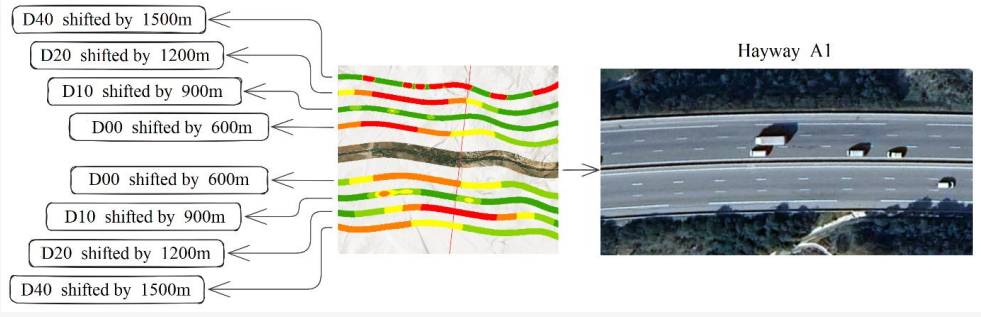

Figure 15: Spatial representations of pavement defect concentration using the Kernel Density Estimation (KDE)

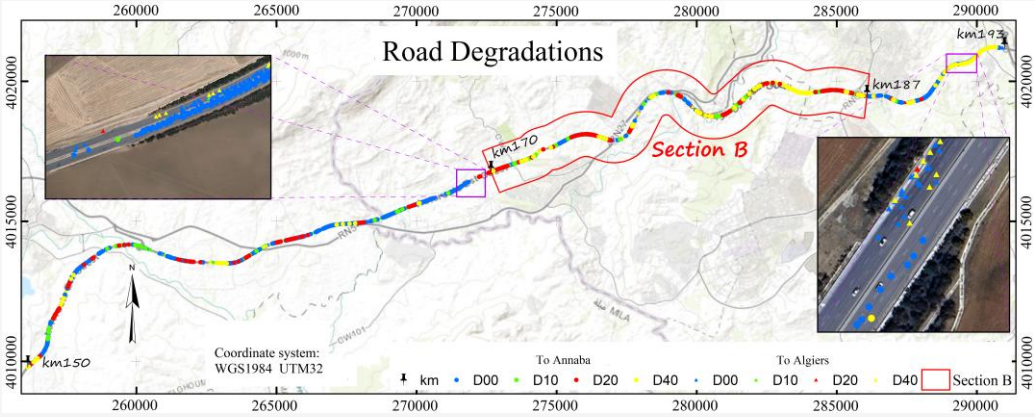

Figure 16: Defects geolocated and classed into four types

3. Results and Discussion

Road Analyzer recorded four files (avv1 to avv4), containing 11 694 geolocated and classified defects (Figure 16). Table 3 presents the number of defects by class, distributed according to the two directions (Annaba to Algiers, Algiers to Annaba).

Table 3: Number of geolocated defects by class

Class	Annaba to Algiers	Algiers to Annaba
D00	3008 [64%]	5305 [76%]
D10	465 [10%]	963 [14%]
D20	233 [5%]	412 [6%]
D40	975 [21%]	333 [5%]
Total	4681 [100%]	7013 [100%]

3.1 Interpretation by Class

The table shows that longitudinal defects (D00, minor or superficial defects) are the most frequent in both directions, representing 76% of the defects from Algiers to Annaba and 64% from Annaba to Algiers (Figure 17).

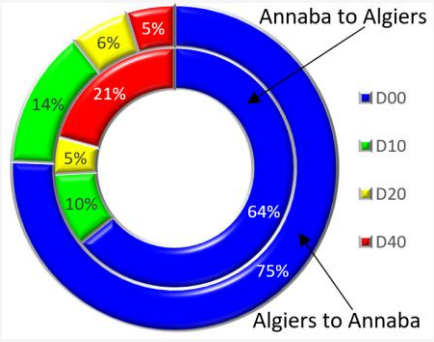

Figure 17: Geolocated defects by class

The D10 and D20 classes, corresponding to transverse cracks and alligator, represent smaller but nonetheless significant proportions. Their higher percentage in the direction from Algiers to Annaba indicates that the pavement in this direction is more degraded. The D40 type is more frequent towards Algiers (975 vs 333), which could reflect a different typology of stress or construction in this direction of traffic. Although the D10, D20, and D40 defects are less frequent, they deserve special attention as they could indicate deeper (structural) defects.

3.2 Overall Comparison of the Two Directions

The total number of defects in the direction from Algiers to Annaba (7013) is significantly higher than in the direction from Annaba to Algiers (4681). This can be explained by:

- Heavier or denser traffic in the West-East direction
- An unfavorable slope or gradient

The imbalance between the two directions suggests the need to analyze the geometric conditions (slope, curve radius), heavy vehicle traffic (trucks), as well as the dates of intervention and maintenance.

3.3 Comparative Analysis by Sections

The number of defects for the two studied sections is presented in Table 4 and Figure 18.

According to the total number of defects

Table 4 and Figure 16 show that the number of geolocated defects in Section B (6057) exceeds that recorded in Section A (5637), despite Section B being almost half as long. This indicates that the defects are more spatially concentrated in Section B.

According to the defect density per km

Table 4 shows that the density in Section B is nearly double that of Section A. This constitutes a clearly unfavorable indicator for section B, which has a flexible structure, in terms of long-term durability and performance. The high defect density in section B indicates lower structural performance, despite a theoretically greater thickness (Figure 3).

Table 4: Number of geolocated defects by section

Section	D00	D10	D20	D40	Total	Length(km)	Density (defects/km)
A	4,341	350	104	842	5,637	28	201/km
B	3,972	1,078	541	466	6,057	15.36	394/km
Total	8,313	1,428	645	1,308	11,694	43.36	270/km

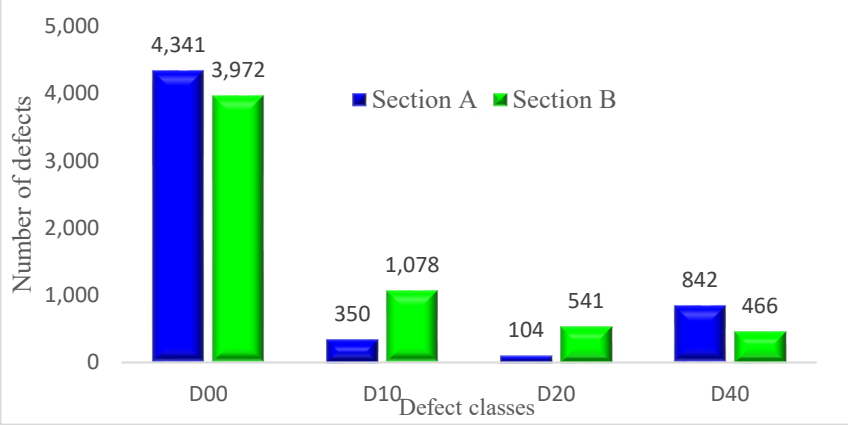

Figure 18: Geolocated defects by section

Table 5: Number of defects by commissioning date

Section	Pavement structure type	Commis-sioning Date	Lenth (km)	Age in 2023 (years)	Number of defects	Defects/Year	Defects/km/year
A	Semi-rigid	July 2010	26	13	5,637	435	16.67
B	Flexible	2006	15.36	17	6,057	356	23.2

3.4 Analysis According to the Commissioning Date

The statistics calculated and recorded in Table 5 show that Section A exhibits a faster rate of defect (435 defects per year) compared to Section B (356 defects per year). However, this result does not fully reflect reality, as it does not account for the length of each section. The indicator that takes this information into account is presented in the last column of the table, which shows the number of defects per km per year. This indicator is essential for assessing the durability and structural performance of each type of pavement. Consequently, the results indicate that Section B degrades more rapidly than Section A, with a defect rate that exceeds Section A by 6.53 defects/km/year.

3.5 Validation

The confusion matrix and the corresponding evaluation report, calculated by the implemented program, are illustrated in Figure 19 and Table 6 respectively. Table 6 presents an F1-score of 93.27%, indicating a high overall performance of the approach, demonstrating a robust capability to accurately identify and localize the different types of defects. A recall of 91.81% underscores the effectiveness of the approach in detecting the majority of the defects present in the data, while minimizing false negatives. Additionally, a precision of 95.53% reflects the reliability of the system's detections, showing that the predicted defects largely align with the actual observed defects, thereby reducing false positives.

Beyond these values, Table 6 also reports the *support* associated with each class, representing the number of validation samples per defect category. This indicator is essential to interpret class-wise behavior: categories with lower support, such as D20 (17 samples) or D40 (16 samples), may show performance variations due to limited representativeness. Nevertheless, visually distinctive classes may still achieve high accuracy even under small support, as observed for D40. Despite these differences in class support, the Overall Accuracy (OA) of 93.57% confirms that most road surface points are correctly classified. However, OA can be misleading in the presence of class imbalance, as majority classes contribute more to the overall score; therefore, the macro-F1 score of 93.27% provides a complementary measure of balanced performance across all categories.

Table 6: Classification report

Defect class	Precision	Recall	F1-score	Support
ND	0.914	0.941	0.928	34
D00	0.904	1.000	0.9450	47
D10	0.958	0.885	0.920	26
D20	1.000	0.762	0.867	17
D40	1.000	1.000	1.000	16
$Macro_{avg}$	0.955	0.918	0.933	140
OA	0.936			

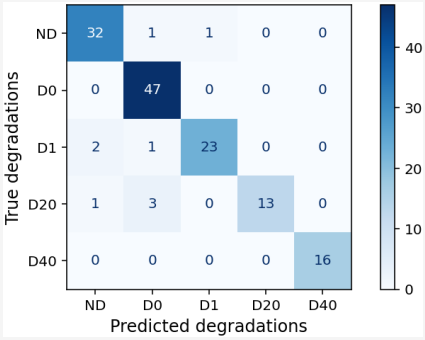

Figure 19: Confusion matrix

Taken together, these metrics underline the robustness of the proposed system. The confusion matrix shows that, among the 34 ND points collected in situ, only 2 points were misclassified by the system, being respectively assigned to the D10 and D00 classes. The defects of type D00, although correctly identified and localized, were associated with a few false positives, primarily originating from the D20 class. Additionally, a D20 defect was not detected and was erroneously classified as non-degraded (ND class). The relatively lower recall of the D20 class observed in Table 6 is explained by the limited number of D20 validation samples (76.47%, based on 17 samples) and the intrinsic ambiguity of this defect category. A D20 defect, of a moderate nature, can be perceived as a combination of D00 and D10 cracks. This characteristic makes its detection more complex; consequently, the system may underestimate or misidentify this type of defect. As a result, the combination of less severe cracks may sometimes be incorrectly classified into a lower category, such as D00, leading to omissions in detecting moderate D20 defects, even though all predicted D20 samples are correctly classified (100% precision).The omission of one D20 defect point as ND does not necessarily indicate a detection failure, but is likely due to the decametric precision of GPS, with the defect located slightly beyond the 10 m matching radius. Although these defects do not present an immediate danger, they may become problematic in the long term if not addressed.

In contrast, the D40 category achieves perfect performance, with precision, recall, and F1-score all equal to 1.00 (100%). This is explained by the morphological clarity of D40 defects, which exhibit well-defined geometry, enabling the system to recognize them without confusion with other defect types. Although the support for this category is relatively small, its homogeneity facilitates effective generalization, as reflected by the absence of misclassified instances in Figure 19. These results confirm the reliability of the proposed approach for detecting the most critical defect types in terms of road safety.

3.6 Mapping

The resulting KDE surfaces were reclassified into five density levels (sound, minor, moderate, major, and severe), represented by a color gradient ranging from green (low density) to red (high density). Eight thematic maps (Figure 20) were produced (four for each traffic direction) and subsequently integrated into a comprehensive synthesis map (Figure 21), illustrating the overall spatial distribution of defects across the studied highway section. In order to distinguish between the two sections studied, Section B is outlined by a red frame on the various maps created, while Section A is located outside of this frame. In the following section, maps have been generated using a spatial clustering approach for the different types of defects (Figure 22, Figure 23, Figure 24 and Figure 25). These maps highlight the areas with the highest concentrations of defects along the highway corridor. The size of the circles is proportional to the number of occurrences of the cracks. Their color ranges from yellow (indicating low concentration) to red (indicating high concentration). Spatial clustering is an effective tool for prioritizing intervention areas and justifying differentiated maintenance strategies.

3.6.1 Longitudinal defects clustering

- Direction Algiers to Annaba (5305 cracks): The clustering of longitudinal cracks (Figure 22) is clearly visible throughout this stretch of road Some areas, particularly those between KP 165 and KP 187, show a particularly high number of cracks (orange and red zones).
- Direction Annaba to Algiers (3008 cracks): Although longitudinal cracks are also present, their clustering appears more scattered in this direction. Light yellow zones (indicating a low number of cracks) are more numerous in this direction, which could suggest a difference in traffic type.
- Focus on section B: Section B is a critical area as numerous red and orange points appear within this section. This reflects a significant concentration of longitudinal cracks in this part of the route. The concentration of defects in specific sections requires priority repairs.

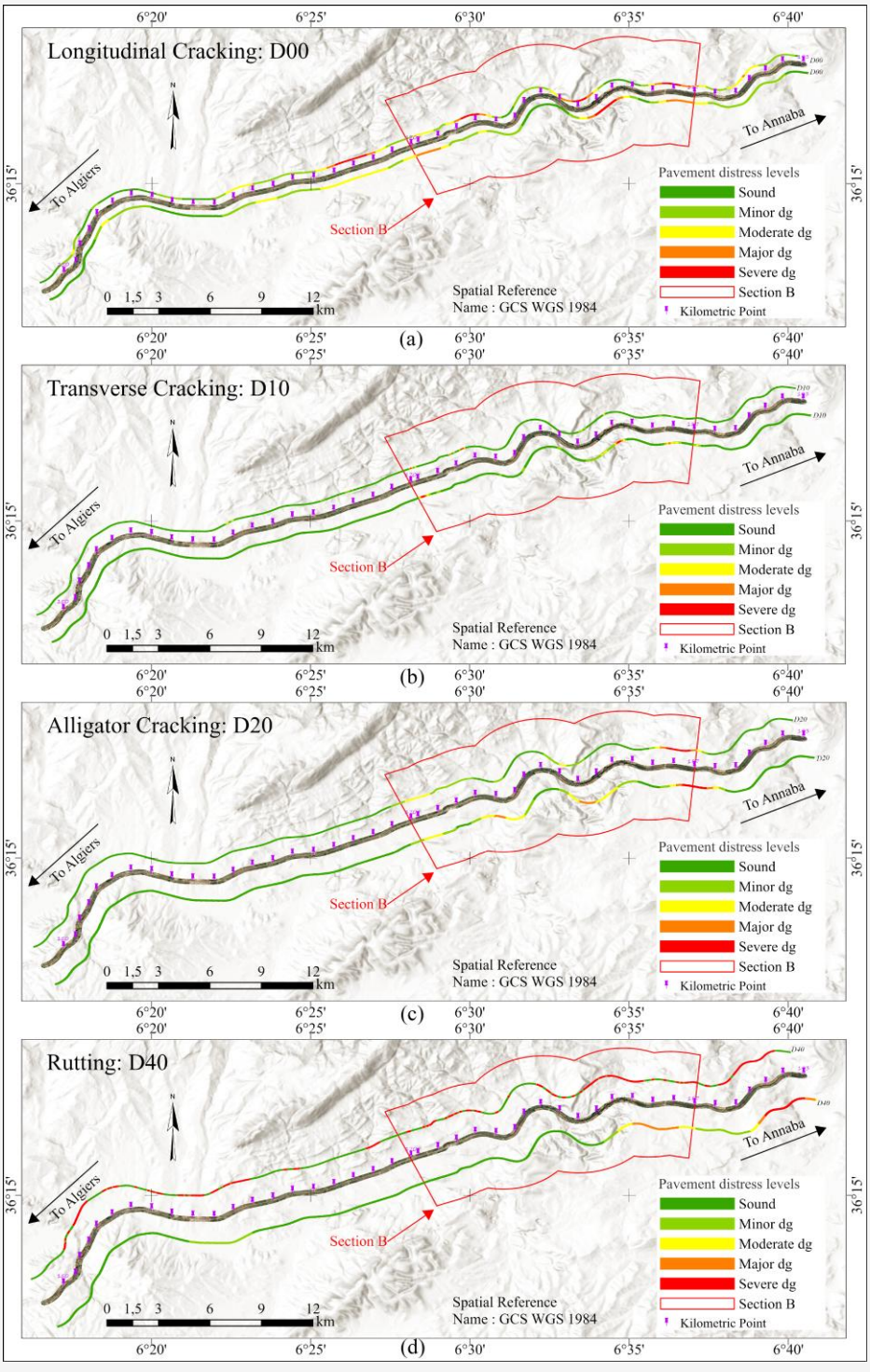

Figure 20: Spatial representations of pavement defect concentration per type
(a) longitudinal cracks (b) transverse cracks (d) alligator cracking and (c) rutting and potholes

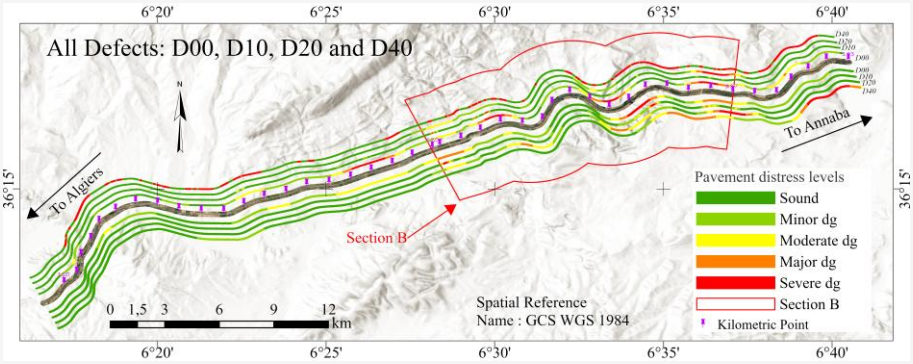

Figure 21: Synthesis map of the spatial distribution of defects along the studied highway section

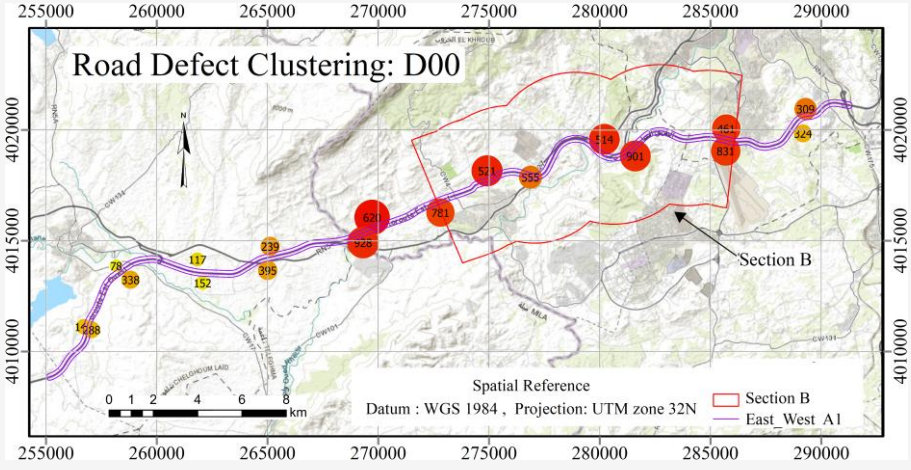

Figure 22: Longitudinal defect clustering

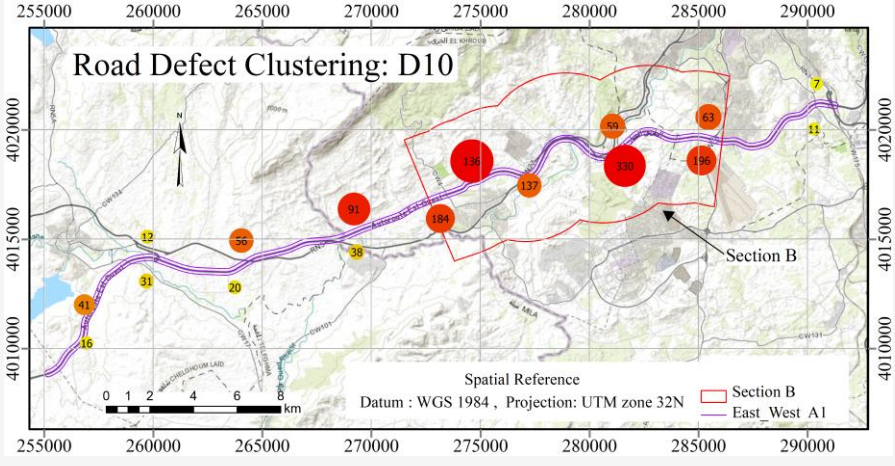

Figure 23: Transversal defect clustering

3.6.2 Transversal defects clustering

- Section A (350 cracks): In this section (Figure 23), the crack clusters are smaller and fewer in number, with values ranging from 12 to 91, evenly distributed. The majority of the clusters are yellow or orange, indicating a low to moderate frequency of cracks.

- Section B (1078 cracks): In contrast to Section A, this section exhibits high concentrations of cracks. Two large red clusters are observed, representing 136 and 330 cases, respectively, along with other clusters in the eastern area, with values of 196, 184, 63, and 59 cases. These clusters reveal a significant vulnerability of this portion of the road to transverse cracks. The effect is localized and asymmetrical,

with areas of high concentration in a restricted perimeter, indicating more specific and severe structural problems in certain areas of this section.

These results indicate that Section A is generally less affected by transverse cracks, confirming its better mechanical performance, while Section B suffers from an accumulation of these cracks, requiring a targeted curative intervention.

3.6.3 Alligator defects clustering

A high density of cracking (541 cases) is clearly observed in Section B (Figure 24) which contains the largest clusters: 108, 92, 90, 88, and 69, indicating significant pavement deterioration in this area. The map also reveals a predominant concentration of defects on the southern side of the highway (from Algiers to Annaba), with 412 cases, while the northern side of the pavement, corresponding to the direction from Annaba to Algiers, shows much less cracking (233 cases), with smaller and fewer circles. Consequently, the pavement in the direction from Algiers to Annaba is more affected by D20 defects than in the opposite direction.

3.6.4 Rutting defects clustering

The comparative analysis reveals a notable asymmetry in the distribution of D40 cracks between the two directions of traffic (Figure 25), with more significant stress observed in the direction from Annaba to Algiers. The spatial study highlights a more dispersed distribution of deformed areas in this direction, characterized by isolated concentration points, indicating a less widespread but locally more pronounced defect. These defects tend to concentrate in areas with complex geological or topographical profiles, particularly on sections with slopes greater than 6%, such as those located between KP 154 and KP 155, KP 182 and KP 184, as well as from KP 190 to KP 192. In contrast, the central portion of the corridor appears relatively unaffected, while the eastern part exhibits increased vulnerability.

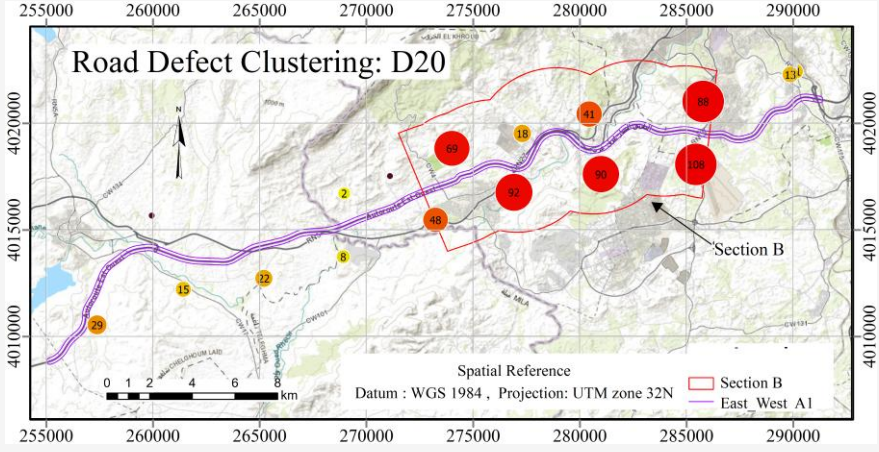

Figure 24: Alligator defect clustering

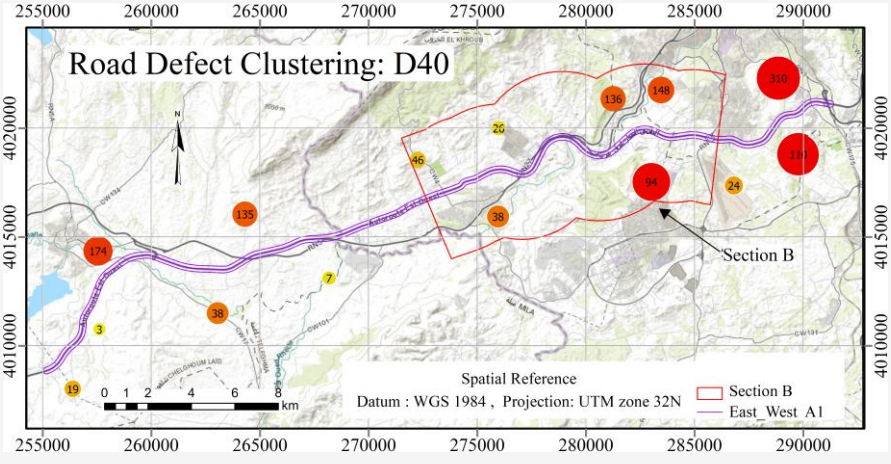

Figure 25: Rutting and potholes defect clustering

4. Conclusion

The approach proposed in this article relies on a simple, secure, easy-to-implement, and low-cost smartphone-based method, utilizing the various sensors embedded in a basic smartphone to automatically detect, identify, and geolocate road defects. The key contributions and novelty of this study lie in demonstrating the operational feasibility of a low-cost photogrammetric workflow for road surface assessment. Unlike UAV- or LiDAR-based techniques, which are limited by high costs, regulatory constraints, and weather dependence, the proposed approach combines smartphone imaging, photogrammetric processing, and georeferencing to provide a rapid, safe, and cost-effective solution for mapping and measuring pavement defects. Importantly, unlike most existing smartphone-based studies, the precise geolocation of defects is integrated into the deliverables, enhancing their practical utility. This methodology balances accuracy, deployability, and speed, offering a flexible and practical alternative for large-scale, real-world infrastructure monitoring.

The methodology adopted relies on the use of deep learning, tested and validated on different datasets, with a performance exceeding 77%. The results obtained on the studied East-West highway section are promising and have been confirmed by in situ measurements. The F1 score of 93.27% demonstrates the robustness and performance of this approach. The proposed system also relies on a photogrammetric approach, which involves decimating the videos into multiple frames. The synchronization of data simultaneously acquired by the various sensors, combined with GPS position estimation, allowed for the reprojection of these images into a terrestrial reference frame. This photogrammetric approach thus enabled the geolocation of the defects with sub-meter precision, while the measurement accuracy reached a centimeter level. The final phase of this work involved the mapping of the defects, using GIS, which allows for the production of deliverable documents that are easily exploitable, supporting a detailed classification of road sections from healthy to severely affected.

The results from the various processing stages show that the two sections of the highway studied exhibit contrasting levels of defect in both directions. Although section B has a thicker pavement structure (over 14 cm) than section A, it is more affected by various types of defects. The rate of defect per kilometer per year indicates a faster deterioration of section B (+6.53 defects per km per year). This can be attributed to several factors, such as the conditions of implementation during construction, the type of materials used, traffic, and the height of the embankments. Further study is needed to identify the main causes of the deterioration of section B. The mapping allowed for the classification of the sections into five categories for each type of defect, ranging from healthy sections to those severely affected. This classification serves as a valuable decision-support tool for the planning and management of predictive and preventive maintenance, ensuring effective and sustainable intervention on the road infrastructure. Indeed, each type of defect requires a specific curative treatment strategy, tailored to its nature and extent. The obtained maps can be used to feed the maintenance service databases and serve as a reference for planning and prioritizing future interventions. The technique employed in this research is useful for long-term monitoring of the defects in the studied area, thus improving road quality and extending the lifespan of the infrastructure. This contributes to the safety and comfort of users, reduces the risk of accidents caused by the road condition, while promoting smoother traffic, enhancing infrastructure performance, and thereby improving economic connectivity. Despite these advantages, certain limitations remain. Data quality is sensitive to vehicle speed, which must be kept below 90 km/h to avoid motion blur, while geolocation accuracy is constrained by the decametric precision of the smartphone GNSS.

Future work will address these limitations and further enhance the methodology. This includes integrating geodetic GPS to improve positioning precision. The adopted methodology also offers the potential for 3D reconstruction of pavement defects, achievable by adding a second smartphone in parallel to ensure stereoscopic coverage for depth estimation. Additionally, cyclic monitoring of road conditions will be implemented through additional field surveys, allowing the evolution of defects to be tracked over time. These developments are expected to further increase the performance, scalability, and applicability of the proposed methodology for comprehensive road infrastructure monitoring.

References

[1] Bouacha, N., Bouguerra, A. and Bouafia, A., (2023). Improving the Resilience of the Road Network in Algeria: A Comparative Analysis of Flexible, Geosynthetically Reinforced, and Rigid Pavements. *Sustainability*, Vol. 15. https://doi.org/10.3390/su151914426.

[2] Alrajhi, A., Roy, K., Qingge, L. and Kribs, J., (2023). Detection of Road Condition Defects Using Multiple Sensors and IoT Technology: A Review. *IEEE Open Journal of Intelligent Transportation Systems*, Vol. 4, 372-392. https://doi.org/10.1109/OJITS.2023.3237480.

[3] Gharbi, A. and Haddadi, S., (2020). Application of the Mobile GIS for the Improvement of the Knowledge and the Management of the Road Network. *Applied Geomatics*, Vol. 12. 23-39. https://doi.org/10.1007/s12518-019-00279-2.

[4] Rathee, M., Bačić, B. and Doborjeh, M., (2023). Automated Road Defect and Anomaly Detection for Traffic Safety: A Systematic Review. *Sensors*, Vol. 23. https://doi.org/10.3390/s23125656.

[5] Zhou, Y., Guo, X., Hou, F. and Wu, J., (2022). Review of Intelligent Road Defects Detection Technology. *Sustainability*, Vol. 14. https://doi.org/10.3390/su14106306.

[6] Kim G. and Kim, S., (2024). A Road Defect Detection System Using Smartphones. *Sensors*, Vol. 24. https://doi.org/10.3390/s24072099.

[7] Kheradmandi, N. and Mehranfar, V., (2022). A Critical Review and Comparative Study on Image Segmentation-Based Techniques for Pavement Crack Detection. *Construction and Building Materials*, Vol. 321. https://doi.org/10.1016/j.conbuildmat.2021.126162.

[8] Abdelwahed, S. H., Sharobim, B. K., Wasfey, B. and Said, L. A., (2025). Advancements in Real-Time Road Damage Detection: A Comprehensive Survey of Methodologies and Datasets. *Journal of Real-Time Image Processing,* Vol. 22. https://doi.org/10.1007/s11554-025-01683-1.

[9] Zeng, K., Fan, R. and Tang, X., (2025). Efficient and Accurate Road Crack Detection Technology Based on YOLOv8-ES. *Autonomous Intelligent Systems,* Vol. 5. https://doi.org/10.1007/s43684-025-00091-3.

[10] Estilong, J. and Palaoag, T., (2025). Literature Review on Road Damage Detection and Severity Recognition: Leveraging Computer Vision. *Journal of Information Systems Engineering and Management*, Vol. 10. https://doi.org/10.52783/jisem.v10i5s.670.

[11] Liu, J., Gu, J. and Luo, S., (2022). *Research on Road Crack Detection based on Machine Vision*: 2022 IEEE 6th Advanced Information Technology, Electronic and Automation Control Conference, IAEAC 2022, Beijing, China, October, 03-05, 2022, 543-547. https://doi.org/10.1109/IAEAC54830.2022.9929645.

[12] Zhao, K., Liu, J., Wang, Q., Wu, X. and Tu, J., (2022). Road Damage Detection from Post-Disaster High-Resolution Remote Sensing Images Based on TLD Framework. *IEEE Access*, Vol. 10. https://doi.org/10.1109/ACCESS.2022.3169031

[13] Gao, Y., Cao, H., Cai, W. and Zhou, G., (2023). Pixel-Level Road Crack Detection in UAV remote Sensing Images Based on ARD-Unet. *Measurement*, Vol. 219. https://doi.org/10.1016/j.measurement.2023.113252.

[14] Silva, L. A., Leithardt, V. R. Q., Batista, V. F. L., Villarrubia González, G. and De Paz Santana, J. F., (2023). Automated Road Damage Detection Using UAV Images and Deep Learning Techniques. *IEEE Access*, Vol. 11. https://doi.org/10.1109/ACCESS.2023.3287770.

[15] Ibrahim, H. B., Salah, M., Zarzoura, F. and El-Mewafi, M., (2023). Smart Monitoring of Road Pavement Deformations from UAV Images by Using Machine Learning. *Innovative Infrastructure Solutions,* Vol. 9. https://doi.org/10.1007/s41062-023-01315-2.

[16] Maeda, H., Sekimoto, Y., Seto, T., Kashiyama, T. and Omata, H., (2018). Road Damage Detection and Classification Using Deep Neural Networks with Smartphone Images," *Computer-Aided Civil and Infrastructure Engineering*, Vol. 33. https://doi.org/10.1111/mice.12387.

[17] Pascucci, N., Dominici, D. and Habib, A., (2025). LiDAR-Based Road Cracking Detection: Machine Learning Comparison, Intensity Normalization, and Open-Source WebGIS for Infrastructure Maintenance. *Remote Sensing,* Vol. 17. https://doi.org/10.3390/rs17091543.

[18] Tessema, T., Gagliardi, V., Sotoudeh, S., Benedetto, A. and Tosti, F., (2024). Assessing Road Pavements Using Satellite Remote Sensing: Towards Developing Network-Level Pavement Monitoring. *Proceedings of the 10th International Conference on Maintenance and Rehabilitation of Pavements, Guimarães, Portugal*, July, 24-26, 2024, Pereira P. and Pais J., Eds., Cham: Springer Nature Switzerland.179-190. https://doi.org/10.1007/978-3-031-63584-7_19.

[19] Chen, C., Chandra, S., Han, Y. and Seo, H., (2022). Deep Learning-Based Thermal Image Analysis for Pavement Defect Detection and Classification Considering Complex Pavement Conditions. *Remote Sensing*, Vol. 14. https://doi.org/10.3390/rs14010106.

[20] Kyriou, A., Mpelogianni, V., Nikolakopoulos, K. and Groumpos, P. P., (2023). Review of Remote Sensing Approaches and Soft Computing for Infrastructure Monitoring. *Geomatics*, Vol. 3. https://doi.org/10.3390/geomatics3030021.

[21] Abrudan, D., Drăgulinescu, A.M. and Vizireanu, N., (2024). Applications of Mathematical Morphology Operators in Civil Infrastructures. *Earth Science Informatics,* Vol. 17. https://doi.org/10.1007/s12145-024-01379-3.

[22] Abrudan, D., (2025). TRIB Crack Dataset: Automatic Recognition System for Road Cracks Detection. *Earth Science Informatics*. Vol. 18. https://doi.org/10.1007/s12145-025-01763-7.

[23] Nasrallah, A. A., Abdelfatah, M. A., Attia, M. I. E. and El-Fiky, G. S., (2024). Positioning and Detection of Rigid Pavement Cracks Using GNSS Data and Image Processing. *Earth Science Informatics*, Vol. 17. https://doi.org/10.1007/s12145-024-01228-3.

[24] Alqaydi, S., Zeiada, W., El Wakil, A., Alnaqbi, A. J. and Azam, A., (2024). A Comprehensive Review of Smartphone and Other Device-Based Techniques for Road Surface Monitoring. *Eng.*, Vol. 5. https://doi.org/10.3390/eng5040177.

[25] Maeda, H., Kashiyama, T., Sekimoto, Y., Seto, T. and Omata, H., (2021). Generative Adversarial Network for Road Damage Detection. *Computer-Aided Civil and Infrastructure Engineering*, Vol. 36. https://doi.org/10.1111/mice.12561.

[26] Arya, D., Maeda, H., Kumar Ghosh, S., Toshniwal, D., Mraz, A., Kashiyama, T. and Sekimoto, Y., (2021). Deep Learning-Based Road Damage Detection and Classification for Multiple Countries. *Automation in Construction*, Vol. 132. https://doi.org/10.1016/j.autcon.2021.103935.

[27] Arya, D., Maeda, H., Ghosh, S. K., Toshniwal, D. and Sekimoto, Y., (2024). RDD2022: A Multi-National Image Dataset for Automatic Road Damage Detection. *Geoscience Data Journal*, Vol. 11. https://doi.org/10.1002/gdj3.260.

[28] Lee, T., Chun, C. and Ryu, S. K., (2021). Detection of Road-Surface Anomalies Using a Smartphone Camera and Accelerometer. *Sensors*, Vol. 21. https://doi.org/10.3390/s21020561.

[29] Mezhoud, S., Clastres, P., Houari, H. and Belachia, M., (2016). Forensic Investigation of Causes of Premature Longitudinal Cracking in a Newly Constructed Highway with a Composite Pavement System *Journal of Performance of Constructed Facilities*. Vol. 31. https://doi.org/10.1061/(ASCE)CF.1943-5509.0000956.

[30] Boukerch, I., Takarli, B., Saidi, K., Kariche, M. and Meguenni, M., (2021). Development of Panoramic Virtual Tours System Based on Low-Cost Devices. *The International Archives of the Photogrammetry, Remote Sensing and Spatial Information Sciences*, Vol. XLIII-B2-2021. https://doi.org/10.5194/isprs-archives-XLIII-B2-2021-869-2021.

[31] As Sami, A. A., Sakib, S., Deb, K. and Sarker I. H., (2023). Improved YOLOv5-Based Real-Time Road Pavement Damage Detection in Road Infrastructure Management. *Algorithms*, Vol. 16. https://doi.org/10.3390/a16090452.

[32] Kariche, I. and Fizazi, H., (2025). Synergistic Exploration Combining Traditional and Evolutionary Methods to Improve Supervised Satellite Images Classification. *International Journal of Computing and Digital Systems*, Vol. 17. http://dx.doi.org/10.12785/ijcds/1571027104.